

# Electrochemical Determination of Paracetamol Using MXene/single-walled Carbon Nanohorns Composite as Sensor

Wei Zhong<sup>1</sup>, Jing Yang<sup>1</sup>, Yansha Gao<sup>1</sup>, Xiaoqiang Wang<sup>1,\*</sup>, Shuwu Liu<sup>1</sup>,  
Mingfang Li<sup>1,\*</sup>, Limin Lu<sup>1,3,\*</sup>, Xuemin Duan<sup>2</sup>

<sup>1</sup> Key Laboratory of Crop Physiology, Ecology and Genetic Breeding, Ministry of Education, Key Laboratory of Chemical Utilization of Plant Resources of Nanchang, College of Science, Jiangxi Agricultural University, Nanchang 330045, PR China

<sup>2</sup> Jiangxi Provincial Key Laboratory of Drug Design and Evaluation, School of Pharmacy, Jiangxi Science and Technology Normal University, Nanchang 330013, PR China

<sup>3</sup> School of Chemistry and Molecular Engineering, Qingdao University of Science and Technology, Qingdao 266042, Shandong, PR China

\*E-mail: [lulimin816@hotmail.com](mailto:lulimin816@hotmail.com)

Received: 7 August 2021 / Accepted: 12 September 2021 / Published: 10 October 2021

---

In this study, single-walled carbon nanohorns (CNHs)-intercalated MXene (Ti<sub>3</sub>C<sub>2</sub>) (MXene/CNHs) composite was successfully synthesized, which was used as electrochemical sensor for paracetamol (PAR) detection. The composite of MXene/CNHs exhibits excellent conductivity, large specific surface area and superior electrocatalytic properties. Specifically, the embedding of the CNHs into MXene nanosheets successfully prevents the re-stacking of MXene and provides abundant active sites for catalytic PAR oxidation, which can availably improve the current signal of the electrochemical sensor. Under the optimum conditions, the designed MXene/CNHs electrode can be employed to detect PAR in a broad concentration range of 5.0 nM - 10.0 μM with a low limit of detection (LOD) of 2.0 nM (S/N = 3). Additionally, the modified electrode exhibits high selectivity, good reproducibility and acceptable stability.

---

**Keywords:** MXene; Single-walled carbon nanohorns; Paracetamol; Electrochemical determination

## 1. INTRODUCTION

Paracetamol (PAR) is widely used as a pharmaceutical pain reliever. It can be used for arthralgia, postoperative pain, neuralgia, and toothache [1-2]. However, excessive and long-term use of PAR produces toxic metabolite accumulation that will result in severe liver damage [3]. Thus, it is urgent to exploit an effective method for monitoring the content of PAR. So far, the commonly used methods for PAR detection include chromatography, chemiluminescence, fluorescence spectroscopy and electrochemical methods [4-7]. Electrochemical strategy gets the favour of many researchers

owing to its low cost, easy operation, rapid response, excellent sensitivity and selectivity [8-10]. At present, various electrode materials, such as N-doped graphene quantum dots/BiOBr [11], Polyimide-multiwall carbon nanotube [12] and Pd/graphene oxide [13] have been utilized to detect PAR. Although these modified electrodes are available for the determination of PAR, the detection sensitivity still needs to be further enhanced. Therefore, the exploration of novel electrode materials with high catalytic performance to detect PAR is highly desired.

As a new family of 2D materials, MXenes obtained via etching of the A-layers from  $M_{n+1}AX_n$  (MAX) phases selectively have attracted increasing research interest as electrode materials because of their high electronic conductivity, surface hydrophilicity and electronegativity [14,15]. However, MXene nanosheets are easy to be restacked because of van der Waals interactions and hydrogen bond, resulting in substantial loss of the active surface area [16]. To avoid MXene from aggregation, some carbon nanomaterials, such as carbon nanotubes (CNTs) and graphene (GR) were proposed as the interlayer spacers [17,18]. Such carbon material-intercalated MXene composites were employed as electrochemical sensing platforms for effective determination of carbendazim,  $H_2O_2$ , hydroquinone, catechol,  $Zn^{2+}$  and  $Cu^{2+}$  [19-23]. As another carbon material, CNHs is a horn-shaped sheath composed of single-wall graphene, which has high porosity and excellent electronic conductivity [24]. Thus, CNHs can be considered as an excellent electrode material. For instance, Zhu et al. synthesized a sensor based on CNHs/graphene oxide for determination of 4-nitrochlorobenzene (4-NCB). The CNHs/graphene oxide exhibited excellent electrocatalysis performance toward 4-NCB owing to the synergistic properties of CNHs and graphene oxide [25]. Chen et al. fabricated phosphomolybdic acid/CNHs modified electrode to detect glucose, which exhibited a broad linearity from 0.035 mM to 4.0 mM [26]. Inspired by these works, high-performance electrode materials can be obtained by using CNHs as interlayer spacer of MXene sheets. However, as far as I am concerned, there is no information on the detection of PAR by MXene/CNHs electrode in the literature.

In this work, MXene/CNHs composite has been prepared and employed as a sensing platform for electrochemical PAR detection. The MXene/CNHs composite combines the advantages of both MXene (good conductivity, large surface area) and CNHs (good electrocatalytic performance), which is helpful to realize highly sensitive detection of PAR. The MXene/CNHs modified electrode exhibits superior electrochemical properties with extended linear ranges and low LOD for PAR detection. Furthermore, the modified electrode shows good reproducibility, stability and selectivity. It is worth to notice that the developed sensor was employed to analysis PAR in tablet samples.

## 2. EXPERIMENT

### 2.1 Materials and apparatus

MXene ( $Ti_3C_2$ ) and CNHs were procured from Nanjing XF Nano Co (Nanjing, China). N,N-Dimethylformamide (DMF),  $Na_2HPO_4$ ,  $NaH_2PO_4$ ,  $K_3Fe(CN)_6$ ,  $K_4Fe(CN)_6$  and ethanol were obtained from Vita Reagent Co., Ltd (Shanghai, China).

Scanning electron microscopy (SEM) images were collected on Nova NanoSEM 450. All the electrochemical measurements were carried out on the CHI760E electrochemical workstation, which

used the classical three electrode system, including glassy carbon electrode, platinum wire electrode, and saturated calomel electrode.

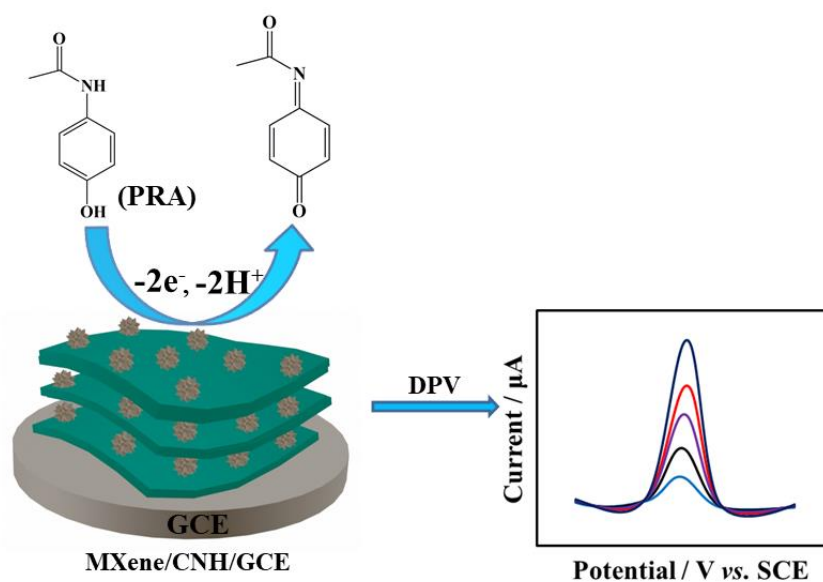
## 2.2 Synthesis of MXene/CNHs composite

To prepare MXene/CNHs composite, CNHs dispersion ( $1 \text{ mg mL}^{-1}$ ) was firstly acquired by dissolving 2 mg CNHs into 2 mL DMF. Then, 1 mL of the prepared CNHs dispersion liquid was added to 1 mL of MXene suspension ( $2 \text{ mg mL}^{-1}$ ). The mixed solution was sonicated for 30 min, which was centrifuged and dried to obtain the MXene/CNHs composite.

## 2.3 Synthesis of modified electrodes

Before the modification, bare glassy carbon electrode (GCE, 3 mm diameter) were polished by  $0.05 \mu\text{m Al}_2\text{O}_3$  slurry on smooth cloth and sonicated subsequently in water.

2 mg MXene/CNHs was dispersed into 2 mL DMF to form uniform dispersion. Then, 5  $\mu\text{L}$  of the above dispersion was dropped on the surface of GCE. After drying in air, MXene/CNHs/GCE was formed. MXene/GCE and CNHs/GCE were obtained by the same procedure. The preparation procedure of MXene/CNHs electrode and the sensing strategy are shown in Scheme 1.



**Scheme 1.** Preparation procedure of MXene/CNHs/GCE and the sensing strategy.

## 2.4 Preparation of actual samples

500 mg PAR tablets were ground to powder. Ethanol (25 mL) was added to dissolve the PAR. The above solution was ultrasonically stirred for 0.5 h, and then centrifuged at 10000 rpm for 3 min. Next, the supernate was transferred and diluted 100 fold by PBS (0.1 M, pH 7.0).

### 3. RESULTS AND DISCUSSION

#### 3.1 Characterization

The morphology of the prepared materials was studied by SEM. As displayed in Figure 1A, MXene shows an obvious layered structure similar to accordion, which provides a large surface area for the target molecule. For MXene/CNHs (Figure 1B), it can be observed that CNHs as interlayer spacers are embedded between MXene layers, preventing the reunion of MXene. This indicates that MXene/CNHs composite has been successfully prepared.

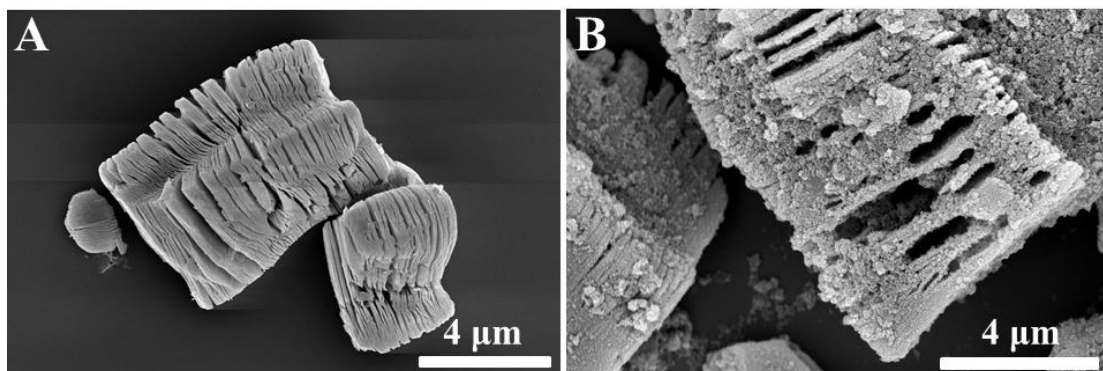


**Figure 1.** SEM images of MXene (A) and MXene/CNHs (B).

#### 3.2 Electrochemical characterizations

Electrochemical impedance spectroscopy (EIS) was utilized to evaluate the interface properties of the modified electrode. In EIS studies, the diameter of the semicircle determines the value of the electron-transfer resistance ( $R_{et}$ ).

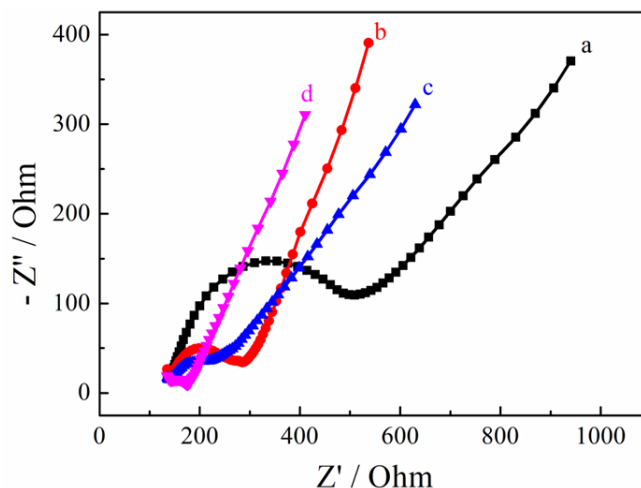


**Figure 2.** EIS of bare GCE (a), MXene/GCE (b), CNHs/GCE (c) and MXene/CNHs/GCE (d) in 5 mM  $K_3Fe(CN)_6/K_4Fe(CN)_6$  (1:1) solution containing 0.1 M KCl.

The Nyquist plots of bare GCE (a), MXene/GCE (b), CNHs/GCE (c) and MXene/CNHs/GCE (d) were shown in Figure 2. The Nyquist plot of the bare GCE (a) consists of a large semicircle, which means a high  $R_{et}$  of bare GCE. For MXene/GCE (b) and CNHs/GCE (c), the  $R_{et}$  values are much smaller than bare GCE, which is because of the good electrical conductivity of MXene and CNHs. After the combination of MXene and CNHs, the  $R_{et}$  of MXene/CNHs/GCE (d) is further decrease. The possible reason is that the combination of CNHs and MXene forms a conductive network, resulting in enhanced electronic conductivity.

### 3.3 Electrochemical behavior of PAR on various electrodes

The electrochemical properties of PAR (10.0  $\mu\text{M}$ ) were investigated using the various modified electrodes in 0.1 M PBS (pH = 7.0) by differential pulse voltammetry (DPV) (Figure 3). For bare GCE (a), there is no oxidation peak, which is attributed to the poor electron-transfer kinetics at the bare GCE. In contrast, obvious oxidation peaks are obtained on MXene/GCE (b) and CNHs/GCE (c). This is owing to the good electronic conductivity and electrocatalytic properties of MXene and CNHs. Moreover, the electrochemical signals of PAR enhance significantly at MXene/CNHs/GCE (d). The excellent performance is because that the introduction of CNHs can prevent the stack of MXene, making more catalytically active sites exposed.

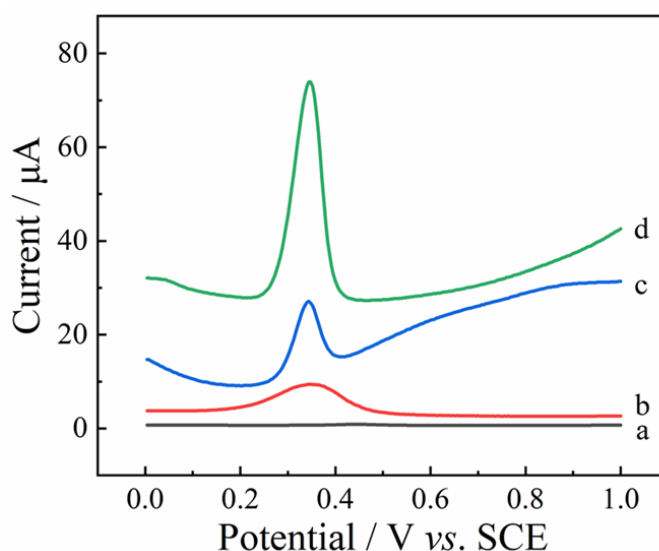


**Figure 3.** DPVs of bare GCE (a), MXene/GCE (b), CNHs/GCE (c) and MXene/CNHs/GCE (d) in 0.1 M PBS (pH 7.0) containing 10.0  $\mu\text{M}$  PAR; Accumulation time: 210 s.

### 3.4 Optimization of the determination conditions

The influence of different pH values (5.0 to 9.0) on the electrochemical behavior to PAR at MXene/CNHs/GCE was investigated by CV. As depicted in Figure 4A, the electrochemical response of PAR enhances as the pH value increasing from 5.0 to 7.0, and obtains a maximum at pH 7.0.

However, the electrochemical response goes down as the pH value increases from 7.0 to 9.0. Thus, the optimum pH value was set as 7.0.

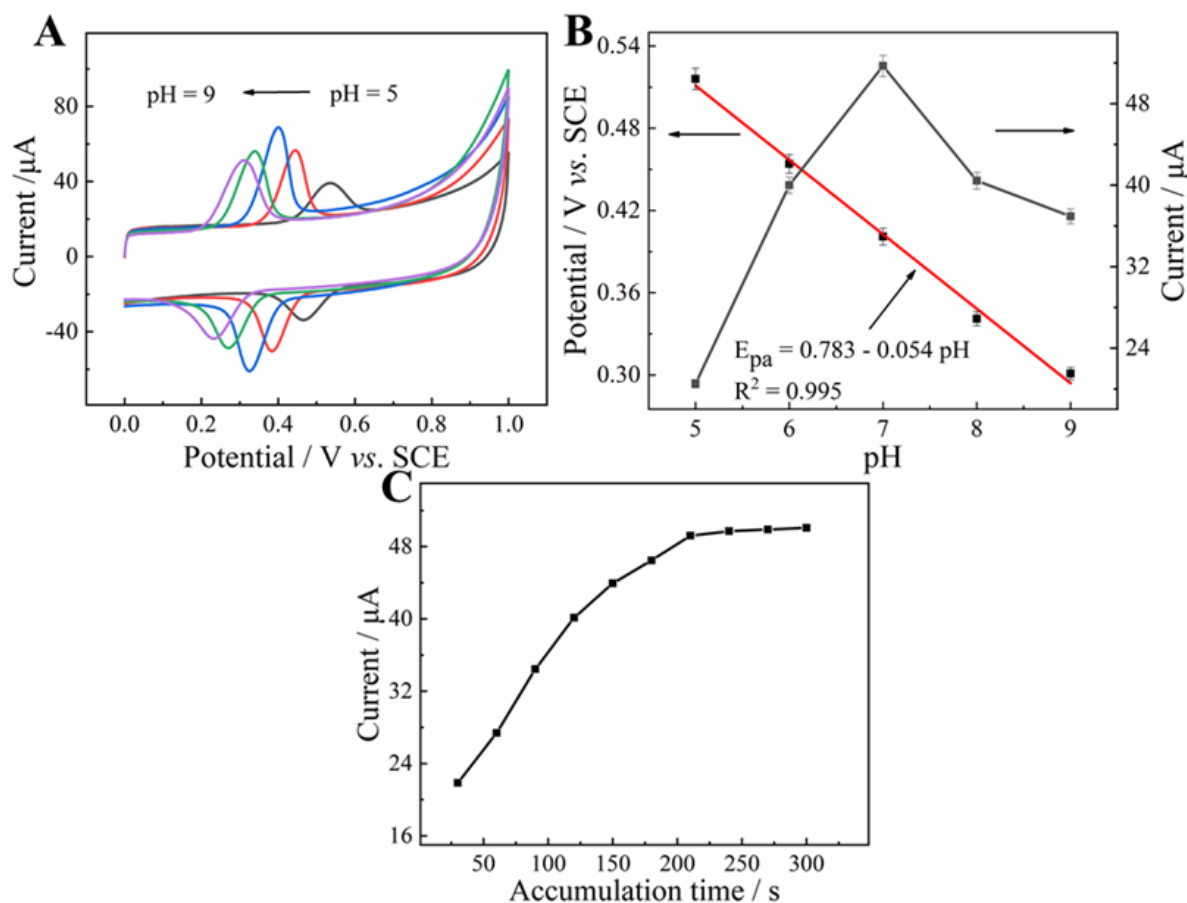


**Figure 4.** (A) CVs of 10.0  $\mu\text{M}$  PAR at MXene/CNHs/GCE with different pH; (B) Effect of pH value on the anodic peak potentials and anodic peak currents; (C) Influence of accumulation time on the peak current of PAR (10.0  $\mu\text{M}$ ) at MXene/CNHs/GCE in 0.1 M PBS (pH 7.0).

In addition, the oxidation potentials move towards negative potentials with pH increased, which indicates that protons participate in the electrode reaction process. Moreover, the oxidation potential ( $E_{\text{pa}}$ ) is directly proportional to the pH with a regression equation of  $E_{\text{pa}} = 0.783 - 0.054 \text{ pH}$  ( $R^2 = 0.995$ ) (Figure 4B). The slope of  $-0.054 \text{ V pH}^{-1}$  is very close to the Nernstian theoretical values ( $-0.059 \text{ V pH}^{-1}$ ), proving that the number of electrons and protons transferred in the reaction is equal [27].

Figure 4C shows the impact of the accumulation time on the electrochemical signal of 10.0  $\mu\text{M}$  PAR ranging from 30 to 330 s. With the extension of accumulation time, the peak current increases gradually and reaches the maximum value at 210 s. While the enrichment time is further extended, the peak current hardly changes, which implied that the adsorption equilibrium was reached on MXene/CNHs/GCE. Therefore, 210 s was chosen as the best enrichment time.

### 3.5 Kinetics studies

To inquiry the kinetic characteristic for the PAR electrocatalytic reactions happened on MXene/CNHs/GCE, the influence of scan rate ( $\nu$ ) on the redox behavior of PAR was shown in Figure 5A. As displayed, peak currents of PAR gradually increase as scan rate increase from 10 to 250  $\text{mV s}^{-1}$ . Moreover, the redox peak currents ( $I_p$ ) are linear dependent on the  $\nu$  (Figure 5B). The equations of linear regression are expressed as:  $I_{pa} (\mu\text{A}) = 0.335 \nu + 3.012$  ( $R^2 = 0.994$ ) and  $I_{pc} (\mu\text{A}) = -0.273 \nu - 0.018$  ( $R^2 = 0.997$ ). This indicates that the redox process of PAR on MXene/CNHs/GCE is an adsorption control process [28].

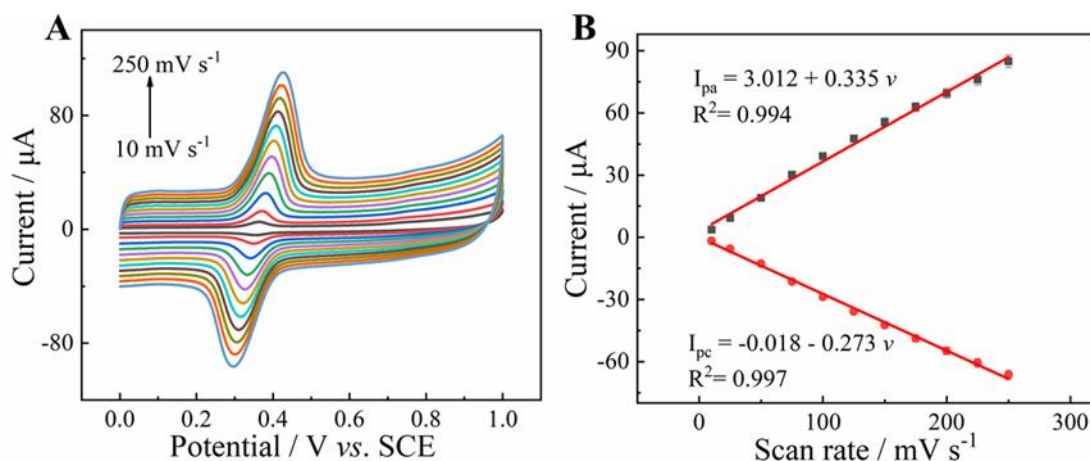


**Figure 5.** (A) CVs of 10  $\mu\text{M}$  PAR on MXene/CNHs/GCE in 0.1 M PBS (pH 7.0) at different scan rates: 10, 25, 50, 75, 100, 125, 150, 175, 200, 225 and 250  $\text{mV s}^{-1}$ ; (B) Linear relationship between the  $I_p$  and the  $\nu$ .

### 3.4 Determination of PAR on the MXene/CNHs/GCE

To evaluate the feasibility of MXene/CNHs/GCE, different concentrations of PAR were detected via DPV under the optimized conditions. The corresponding DPV curves were shown in Figure 6A. With the increase of the PAR concentrations from 5.0 nM to 10.0  $\mu\text{M}$ , the electrochemical signals of PAR are linearly strengthened. The relationships can be described as follows:  $I = 2.074 + 5.054 c$  ( $R^2 = 0.993$ ) (Figure 6B). The LOD is evaluated to be about 2.0 nM. Table 1 displays a performance comparison with the previously reported PAR sensors [29-33]. As shown, MXene/CNHs/GCE exhibits a lower LOD and wider linear range, which can be attributed to the favorable electron transfer and satisfactory electro-catalytic activity endowed by MXene and CNHs.

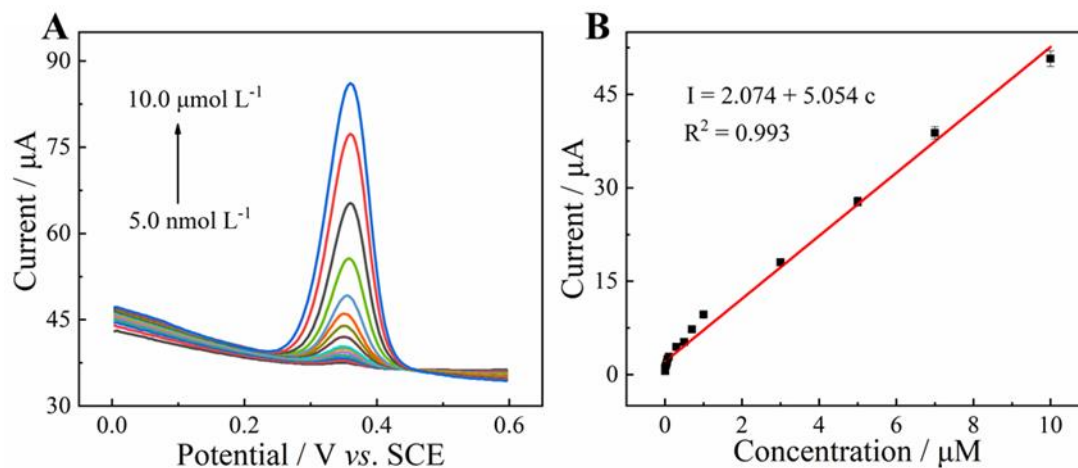


**Figure 6.** (A) DPV of 0.005, 0.05, 0.1, 0.3, 0.5, 0.7, 1.0, 3.0, 5.0, 7.0 and 10.0 μM PAR at MXene/CNHs/GCE in 0.1 M PBS (pH 7.0); (B) Linear curve of oxidation peak current vs. concentration.

**Table 1.** Performance comparison of the MXene/CNHs/GCE with other PAR electrochemical sensors.

Modified electrodes	Method	Linear range	LOD	Reference
ZIF-67/GCE	DPV	2-45 μM	460 nM	[29]
CNT/CPE	DPV	1-1000 μM	38 nM	[30]
MWCNT/GCE	DPV	3-300 μM	10 nM	[31]
ZrO <sub>2</sub> /CPE	DPV	1-2500 μM	912 nM	[32]
MoS <sub>2</sub> /TiO <sub>2</sub> /GCE	SWV	0.5-750 μM	10 nM	[33]
MXene/CNHs/GCE	DPV	0.005-10 μM	2.0 nM	This work

### 3.5 Selectivity, reproducibility and stability

The potential influence of some interference was explored to estimate the selectivity of the method. The results show that 100-fold concentrations of Na<sup>+</sup>, K<sup>+</sup>, Fe<sup>3+</sup>, NO<sub>3</sub><sup>-</sup>, Cl<sup>-</sup> and SO<sub>4</sub><sup>2-</sup>, 50-fold concentrations of dopamine (DA), ascorbic acid (AA) and glucose (GLU) do not interfere the detection signal of PAR (Figure 7). The changes of peak current are below 5%, demonstrating the satisfying selectivity of MXene/CNHs/GCE.

The reproducibility of the sensor was surveyed on one MXene/CNHs/GCE in PBS (0.1 M, pH 7.0) with PAR (10.0 μM) for 20 times continuously via DPV. The relative standard deviation (RSD) of is 4.13%, meaning an excellent reproducibility of the sensor. The stability of MXene/CNHs/GCE was also investigated by intermittent detection of PAR. The oxidation peak currents for 10.0 μM PAR was recorded every 2 days. After one month, the current response of PAR sensor still keeps above 95.6% of the original value, which indicates that MXene/CNHs modified electrode has outstanding stability.

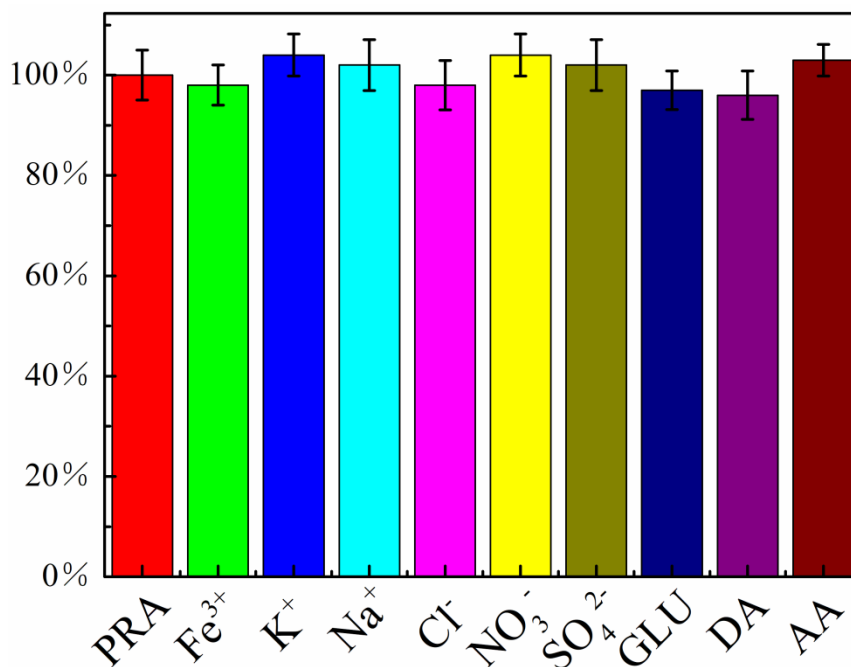


**Figure 7.** Influence of coexisting substances on the current response for PAR by MXene/CNHs/GCE in 0.1 M PBS (pH 7.0) containing 10.0  $\mu\text{M}$  PAR and several interferences (100-fold concentrations of  $\text{Na}^+$ ,  $\text{K}^+$ ,  $\text{Fe}^{3+}$ ,  $\text{NO}_3^-$ ,  $\text{Cl}^-$  and  $\text{SO}_4^{2-}$ , 50-fold of concentrations dopamine (DA), ascorbic acid (AA), glucose (GLU)).

### 3.6 Real sample analysis

To establish the PAR practical ability of the proposed sensor, it was applied to detect PAR in real samples by standard addition method. Details of pretreatment of PAR samples are provided in Section 2.4. As illustrated in Table 2, the recoveries obtained in PAR samples vary from 96.3% to 104.3%. These results suggest MXene/CNHs/GCE is highly accurate and feasible for PAR detection.

**Table 2.** Determination of PAR in real samples (n = 3).

Samples	Added ( $\mu\text{M}$ )	Found ( $\mu\text{M}$ )	RSD (%)	Recovery (%)
1	0.00	0.780	3.7	-
2	3.00	3.64	3.3	96.30
3	5.00	6.03	2.9	104.3
4	10.0	10.6	3.1	98.33

## 4. CONCLUSIONS

Herein, MXene/CNHs electrode was proposed as a new electrochemical platform for sensing of PAR. The as-prepared MXene/CNHs exhibits highly catalytic activity toward PAR oxidation, which is attributed to the large specific surface area and high electronic transmission efficiency of MXene, as well as the excellent catalytic performance of CNHs. The developed PAR sensor shows a wide linear

range of 5.0 nM to 10.0  $\mu$ M, with a low LOD of 2.0 nM. Furthermore, the MXene/CNHs/GCE displays high stability, good reproducibility and acceptable recoveries from 96.3% to 104.3%. All these good electrochemical properties indicate the developed sensor can serve as promising electrochemical sensing platform.

#### ACKNOWLEDGEMENTS

We are grateful to the National Natural Science Foundation of China (51862014, 22064010, 31960499, and 21665010), the Natural Science Foundation of Jiangxi Province (20202ACBL213009 and 20192BBEL50029), Provincial Projects for Postgraduate Innovation in Jiangxi (YC2020-S238), College Students' innovation and entrepreneurship training program (202010410228), Jiangxi Provincial Department of Education (GJJ200430, GJJ200460 and GJJ200429), and Natural Science Foundation of Nanchang City (No. 2018CXTD014) for their financial support of this work.

#### References

1. J. Wang, H. Zhang, J. Zhao, R. Zhang, N. Zhao, H. Ren, Y. Li, *Microchim. Acta*, 186 (219) 1.
2. Y. Song, Y. Zhang, J. Li, C. Tan, Y. Li, *J. Electroanal. Chem.*, 865 (2020) 114157.
3. Y. Teng, L. Fan, Y. Dai, M. Zhong, X. Lu, X. Kan, *Biosens. Bioelectron.*, 71 (2015) 137.
4. W. Ruengsitagoon, S. Liawruangrath, A. Townshend, *Talanta*, 69 (2006) 976.
5. E. A. Abdelaleem, I. A. Naguib, E. S. Hassan, N. W. Ali, *J. Pharm. Biomed. Anal.*, 114 (2015) 22.
6. D. Easwaramoorthy, Y. C. Yu, H. J. Huang, *Anal. Chim. Acta*. 439 (2001) 95.
7. P. V. Narayana, T. M. Reddy, P. Gopal, G. R. Naidu, *Anal. Methods*, 6 (2014) 9459.
8. F. Gao, X. Tu, X. Ma, Y. Xie, J. Zou, X. Huang, F. Qu, Y. Yu, L. Lu, *Talanta*, 215 (2020) 120891.
9. X. Qiu, L. Lu, J. Leng, Y. Yu, W. Wang, M. Jiang, L. Bai, *Food Chem.*, 190 (2016) 889.
10. F. Gao, Y. Yang, X. Tu, Y. Yu, L. Shu, M. Li, Y. Sha, X. Wang, L. Lu, *Synth. Met.*, 277 (2021) 116769.
11. K. Gao, X. Bai, Y. Zhang, Y. Ji, *Electrochim. Acta*, 318 (2019) 422.
12. M. Burc, S. Köytepe, S. T. Duran, N. Ayhan, B. Aksoy, T. Seçkin, *Measurement*, 151 (2020) 107103.
13. J. Li, J. Liu, G. Tan, J. Jiang, S. Peng, M. Deng, Y. Liu, *Biosens. Bioelectron.*, 54 (2014) 468.
14. W. Zheng, P. Zhang, J. Chen, W. B. Tian, Y. M. Zhang, Z. M. Sun, *J. Mater. Chem. A.*, 6 (2018) 3543.
15. W. Zhong, F. Gao, J. Zou, S. Liu, M. Li, Y. Gao, Y. Yu, X. Wang, L. Lu, *Food Chem.*, 360 (2021) 130006.
16. X. Tu, F. Gao, X. Ma, J. Zou, Y. Yu, M. Li, F. Qu, X. Huang, L. Lu, *J. Hazard. Mater.*, 396 (2020)122776
17. X. Li, X. Yin, M. Han, C. Song, H. Xu, Z. Hou, L. Cheng, *J. Mater. Chem. C*, 5 (2017) 4068.
18. J. Yan, C. E. Ren, K. Maleski, C. B. Hatter, B. Anasori, P. Urbankowski, A. Sarycheva, Y. Gogotsi, *Adv. Funct. Mater.*, 27 (2017) 1701264.
19. D. Wu, M. Wu, J. Yang, H. Zhang, K. Xie, C. T. Lin, L. Fu, *Mater. Lett.*, 236 (2019) 412.
20. R. Ramachandran, C. Zhao, M. Rajkumar, K. Rajavel, P. Zhu, W. Xuan, F. Wang, *Electrochim. Acta*, 322 (2019) 134771.
21. R. Huang, S. Chen, J. Yu, X. Jiang, *Ecotoxicol. environ. saf.*, 184 (2019) 109619.
22. X. Hui, M. Sharifuzzaman, S. Sharma, X. Xuan, S. Zhang, S. G. Ko, J. Y. Park, *ACS Appl. Mater. Interfaces*, 12 (2020) 48928.
23. L. Lorencova, T. Bertok, J. Filip, M. Jerigova, D. Velic, P. Kasak, J. Tkac, *Sensor. Actuat. B: Chem.*, 263 (2018) 360.

24. Y. Yi, O. J. Kingsford, M. N. Fiston, J. Qian, Z. Liu, L. Liu, G. Zhu, *J. Electroanal. Chem.*, 801 (2017) 38.
25. G. Zhu, H. Sun, B. Zou, Z. Liu, N. Sun, Y. Yi, K. Y. Wong, *Biosens. Bioelectron.*, 106 (2018) 136.
26. J. Chen, P. He, H. Bai, H. Lei, K. Liu, F. Dong, X. Zhang, *J. Electroanal. Chem.*, 784 (2017) 41.
27. T. Gan, J. Sun, S. Cao, F. Gao, Y. Zhang, Y. Yang, *Electrochim. Acta*, 74 (2012) 151.
28. S. L. Yang, G. F. Wang, G. Li, J. J. Du, L. B. Qu, *Electrochim. Acta*, 144 (2014) 268.
29. N. T. T. Tu, P. C. Sy, T. V. Thien, T. T. T. Toan, D. Q. Khieu, *J. Mater. Sci.*, 54 (2019) 11654.
30. M. Mazloun-Ardakani, M. Zokaie, A. Khoshroo, *Ionics*, 21 (2015) 1741.
31. Z. A. Alothman, N. Bukhari, S. M. Wabaidur, S. Haider, *Sensor. Actuat. B: Chem.*, 146 (2010) 314.
32. M. Mazloun-Ardakani, H. Beitollahi, M. K. Amini, F. Mirkhalaf, M. Abdollahi -Alibeik, *Sensor. Actuat. B: Chem.*, 151 (2010) 243.
33. N. Kumar, A. S. Bhadwal, B. Mizaikoff, S. Singh, C. Kranz, *Sens. Bio-Sens. Res.*, 24 (2019) 100288.

© 2021 The Authors. Published by ESG ([www.electrochemsci.org](http://www.electrochemsci.org)). This article is an open access article distributed under the terms and conditions of the Creative Commons Attribution license (<http://creativecommons.org/licenses/by/4.0/>).